

# Approximate Integrals Over Bounded Volumes with Smooth Boundaries

Jonah A. Reeger

Received: date / Accepted: date

**Abstract** A Radial Basis Function Generated Finite-Differences (RBF-FD) inspired technique for evaluating definite integrals over bounded volumes that have smooth boundaries in three dimensions is described. Such methods are necessary in many areas of Applied Mathematics, Mathematical Physics and myriad other application areas. Previous approaches required restrictive uniformity in the node set or a mapping to a more convenient domain of integration, which the algorithm presented here does not require. By using the RBF-FD-like approach, the proposed algorithm computes quadrature weights for  $N$  arbitrarily scattered nodes in only  $O(N \log N)$  operations with tunable orders of accuracy.

**Keywords** Radial Basis Function · RBF · quadrature · volume · ball

**Mathematics Subject Classification (2010)** 68Q25 · 65R99

## 1 Introduction

This article is concerned with the development of a method for the approximate evaluation of definite integrals over bounded volumes that have smooth boundaries in  $\mathbb{R}^3$ . That is, consider volume integration over the domain,  $\Omega$ , where the boundary,  $\partial\Omega$ , is described by, for instance, all points satisfying  $h(\mathbf{x}) \leq 0$ . Here  $h : \mathbb{R}^3 \mapsto \mathbb{R}$  is a smooth function. A key aspect of the algorithm presented here, however, is that the function  $h$  need not be known. All that is required is a tessellation of the domain with tetrahedra.

Approximation of the values of definite integrals is commonly known as quadrature when considering integration over an interval, or quadrature/cubature when

---

This work was funded by the Office of Naval Research program Atmospheric Propagation Sciences for High Energy Lasers and the Air Force Office of Scientific Research project Radial Basis Functions for Numerical Simulation.

---

J. A. Reeger  
United States  
E-mail: jonah.reeger@gmail.com

considering integration occurs over domains in two or more dimensions. Much research has been devoted to developing sophisticated and accurate techniques for estimating the values of integrals over intervals, areas, and volumes with some of the earliest work tracing back many centuries to early attempts to measure the area of the circle [1]. There are many texts devoted to summarizing such methods, see, for example [1, 2, 3, 4].

The problem of evaluating definite integrals over volumes with smooth bounding surfaces is gaining popularity. In particular, attention has recently been paid to improvements to finite element methods in the presence of implicitly defined surfaces, but often with illustrations only in  $\mathbb{R}^2$  [5] or for elements which impose a particular structure on the node sets, e.g. hyperrectangles [6]. These methods can often rely on choosing appropriate coordinate systems for applying Gaussian quadrature over each dimension (see, e.g. [7]). Further, some of these previous methods required explicit knowledge of  $h$  and its derivatives, an unnecessary complication remedied in section 2.4. Other methods for integrating over volumes rely on the Gauss divergence theorem [8] and node sets designed for certain characteristics [9].

Since numerical quadrature is often a follow-up to some other task (such as collecting data or numerically solving Partial Differential Equations (PDEs)), it can be impractical to require node locations that are specific to the quadrature method. It is true that an extra interpolation step could take place to approximate the integrand at node locations specific to the quadrature rule, but this is an unnecessary step that imposes constraints on the compatibility of the accuracy of the interpolation and quadrature. Further, such a step may be unworkable if the interpolation step itself places constraints on the node set. Requirements on node locations are common in, for instance, Newton-Cotes or Gaussian Quadrature rules for evaluating definite integrals of intervals in 1-dimension. In both cases a polynomial interpolant of the integrand is constructed and then integrated, with interpolation conditions enforced at node locations that either have equal spacing between adjacent nodes or are tied to roots of orthogonal polynomials.

To overcome these requirements on the structure of the node set, the present algorithm is designed to find the quadrature weights given a node set defined by the application or user. It is possible to construct a polynomial interpolant of the integrand in this context, followed by integration of the interpolant, in more than one dimension. Unfortunately, however, the polynomial basis set used for interpolation does not depend on the locations of the nodes, and such basis sets suffer from a question of the existence and uniqueness of an interpolant on unstructured node sets [10, 11], which has prompted the use of Radial Basis Functions (RBFs) in the approximation of the integrand.

The numerical method described in this paper is a generalization of RBF-FD (radial basis function-generated finite differences) and an extension of the work in [12], which considered only the volume of the ball in  $\mathbb{R}^3$ , to volumes bounded by arbitrary smooth surfaces. The concept of RBF-FD has been successfully applied to solve PDEs (see [13, 14] for surveys of these applications) and to construct quadrature rules for an interval in one-dimension, bounded domains in two-dimensions and, more specifically, integrals over bounded two-dimensional (piecewise-)smooth surfaces embedded in three-dimensions (see [15, 16, 17] and the references therein).

The following Section 2 describes the present quadrature method. Section 3 describes some test examples, with illustrations of convergence rates and computational costs. Finally, section 4 outlines some conclusions.

## 2 Description of the key steps in the algorithm

Consider evaluating

$$\iiint_{\Omega} f(\mathbf{x})dV, \quad (1)$$

where  $\Omega = \{\mathbf{x} \in \mathbb{R}^3 : h(\mathbf{x}) \leq 0\}$ .

Similar to the work presented in [15, 16, 17] for surface integrals and [12] for the volume of the ball in  $\mathbb{R}^3$ , at a high level, the proposed algorithm can be described in four steps:

1. Decompose the domain of integration into  $K \in \mathbb{Z}^+$  subdomains.
2. On the  $k^{\text{th}}$  subdomain construct an interpolant of the integrand.
3. Integrate the interpolant of the integrand to determine weights for integrating a function  $f$  over the  $k^{\text{th}}$  subdomain.
4. Combine the weights for the integrals over the  $K$  subdomains to obtain a weight set for approximating the volume integral of  $f$  over  $\Omega$ .

Each of these steps is described in greater detail in what follows. Throughout the remainder of this paper, the subscript  $k$  will be used to indicate that the steps are carried out for each tetrahedron separately. When further subscripting is necessary—for instance, to indicate entries of a vector, matrix, or a set—the necessary indexing will follow after a comma. For clarity, much of what is presented in sections 2.1 through 2.3.1 is repeated from [12].

### 2.1 Step 1: Decompose the domain of integration

Suppose that  $\mathcal{S}_N = \{\mathbf{x}_i\}_{i=1}^N$  is a set of  $N$  unique points in  $\Omega$ , with a subset exactly on the boundary surface. On the set  $\mathcal{S}_N$  construct a tessellation  $T = \{t_k\}_{k=1}^K$  (via Delaunay tessellation or some other algorithm) of  $K$  tetrahedra. These tetrahedra encompass the bulk of the volume of  $\Omega$ . However, the tetrahedra near the boundary, with  $h = 0$  on at least three vertices, likely over- or under-approximate the volume locally.

Let  $\mathcal{K}_S \subset \{1, 2, \dots, K\}$  be the set of indices such that if  $k \in \mathcal{K}_S$  then the tetrahedron  $t_k$  has at least one face that is not shared with any of the other tetrahedra, call it  $\tau_{k,*}$ . This face has all three vertices on the surface of  $\Omega$ , i.e.  $h = 0$  on these vertices, and unless the surface is planar there is a sliver of volume,  $s_k$ , between  $\tau_{k,*}$  and the smooth, curved bounding surface that must be accounted for in decomposing the volume. Conversely, let  $\mathcal{K}_I = \{1, 2, \dots, K\} \setminus \mathcal{K}_S$  be the indices of tetrahedra that do not have a face with three vertices on the surface. With these definitions (1) can be decomposed as

$$\iiint_{\Omega} f(\mathbf{x})dV = \sum_{k \in \mathcal{K}_I} \iiint_{t_k} f(\mathbf{x})dV + \sum_{k \in \mathcal{K}_S} \left( \iiint_{t_k} f(\mathbf{x})dV + \nu_k \iiint_{s_k} f(\mathbf{x})dV \right), \quad (2)$$

with  $\nu_k^2 = 1$  and  $\nu_k \in \mathbb{R}$ . The region  $s_k$  can exist entirely inside, entirely outside, or might be partially inside and outside of  $t_k$ . Therefore, to make (2) valid, it is important to choose a coordinate system and  $\nu_k$  so that only portions of  $s_k$  outside of  $t_k$  are added and the remainder is subtracted. A useful way of defining the coordinate system is to locate the origin in the plane containing  $\tau_{k,*}$  and to align two of the coordinate axes so that they are parallel to  $\tau_{k,*}$ . Two such coordinate systems will be defined in section 2.3.2.

## 2.2 Step 2: Construct an interpolant of the integrand

For each tetrahedron in  $T$  define the sets  $\mathcal{N}_k = \{\mathbf{x}_{k,j}\}_{j=1}^n$  to be the  $n$  points in  $\mathcal{S}_N$  nearest to the midpoint,  $m_k$ , of  $t_k$  (the average of the vertices of  $t_k$ ). Then for an individual  $t_k$  the integral

$$\iiint_{t_k} f(\mathbf{x}) dV \quad (3)$$

is evaluated by first approximating  $f(\mathbf{x})$  by an RBF interpolant, with interpolation points from the set  $\mathcal{N}_k$ , and then integrating the interpolant. Often the RBF interpolant is a linear combination of (conditionally-) positive definite RBFs,

$$\phi(\|\mathbf{x} - \mathbf{x}_{k,j}\|_2), j = 1, 2, \dots, n$$

and augmented by multivariate polynomial terms. If  $k \in \mathcal{K}_S$ , then the same interpolant and set of nodes is used for approximating the integrand over  $s_k$ . Define  $\{\pi_l(\mathbf{x})\}_{l=1}^M$ , with  $M = \frac{(m+1)(m+2)(m+3)}{6}$ , to be the set of all of the trivariate polynomial terms up to degree  $m$ . The interpolant is constructed as

$$s(\mathbf{x}) := \sum_{j=1}^n c_{k,j}^{\text{RBF}} \phi(\|\mathbf{x} - \mathbf{x}_{k,j}\|_2) + \sum_{l=1}^M c_{k,l}^p \pi_l(\mathbf{x}),$$

where  $c_{k,1}^{\text{RBF}}, \dots, c_{k,n}^{\text{RBF}}, c_{k,1}^p, \dots, c_{k,M}^p \in \mathbb{R}$  are chosen to satisfy the interpolation conditions  $s(\mathbf{x}_{k,j}) = f(\mathbf{x}_{k,j}), j = 1, 2, \dots, n$ , along with constraints  $\sum_{j=1}^n c_{k,j}^{\text{RBF}} \pi_l(\mathbf{x}_{k,j}) = 0$ , for  $l = 1, 2, \dots, M$ .

## 2.3 Step 3: Integrate the interpolant of the integrand

By integrating the interpolant, the approximation of the integral of  $f$  is reduced to

$$\iiint_{t_k} f(\mathbf{x}) dV \approx \sum_{j=1}^n w_{k,j} f(\mathbf{x}_{k,j})$$

for  $k \in \mathcal{K}_I$  and

$$\iiint_{t_k} f(\mathbf{x}) dV + \nu_k \iiint_{s_k} f(\mathbf{x}) dV \approx \sum_{j=1}^n w_{k,j} f(\mathbf{x}_{k,j})$$

for  $k \in \mathcal{K}_S$ . A simple derivation can be carried out to show that the weights can be found by solving the linear system  $A_k \mathbf{w}_k = \mathbf{I}_k$  with  $(n + M) \times (n + M)$  matrix

$$A_k = \begin{bmatrix} \Phi_k^T & P_k \\ P_k^T & 0 \end{bmatrix}.$$

The  $n \times n$  submatrix  $\Phi_k$  is made up of the RBFs evaluated at each point in  $\mathcal{N}_k$ , that is

$$\Phi_{k,ij} = \phi(\|\mathbf{x}_{k,i} - \mathbf{x}_{k,j}\|), \text{ for } i, j = 1, 2, \dots, n.$$

Likewise the  $n \times M$  matrix  $P_{k,il}$  consists of the polynomial basis evaluated at each point in  $\mathcal{N}_k$  so that

$$P_{k,il} = \pi_l(\mathbf{x}_{k,i}), \text{ for } i = 1, 2, \dots, n \text{ and } l = 1, 2, \dots, M.$$

If  $k \in \mathcal{K}_I$ , the right hand side,  $\mathbf{I}_k$ , includes integrals of the basis functions over  $t_k$  only. That is,

$$I_{k,j} = \begin{cases} \iiint_{t_k} \phi(\|\mathbf{x} - \mathbf{x}_{k,j}\|) dV & j = 1, 2, \dots, n \\ \iiint_{t_k} \pi_{j-n}(\mathbf{x}) dV & j = n + 1, n + 2, \dots, n + M \end{cases}.$$

The integrals of the trivariate polynomial terms can be evaluated exactly via, for instance, the Divergence Theorem or barycentric coordinates. For the RBFs, the integrals can be evaluated by further decomposing  $t_k$  into four tetrahedra that share the common vertex  $\mathbf{x}_{k,j}$ . Summing the integrals of the RBFs over the four tetrahedra results in the integral over  $t_k$ . This process allows the volume integral over a tetrahedron to be reduced to four integrals in a single dimension. Section 2.3.1 explains this process.

On the other hand, for  $k \in \mathcal{K}_S$

$$I_{k,j} = \begin{cases} \iiint_{t_k} \phi(\|\mathbf{x} - \mathbf{x}_{k,j}\|) dV + \nu_k \iiint_{s_k} \phi(\|\mathbf{x} - \mathbf{x}_{k,j}\|) dV & j = 1, 2, \dots, n \\ \iiint_{t_k} \pi_{j-n}(\mathbf{x}) dV + \nu_k \iiint_{s_k} \pi_{j-n}(\mathbf{x}) dV & j = n + 1, \dots, n + M \end{cases}.$$

The integrals over  $t_k$  are evaluated using the methods described in the previous paragraph and in section 2.3.1 while the integrals over  $s_k$  are approximated using a scheme discussed in section 2.3.2.

### 2.3.1 Integrals of RBFs Over Tetrahedra

Suppose that the tetrahedron  $t_k$  has vertices  $\mathbf{a}_k$ ,  $\mathbf{b}_k$ ,  $\mathbf{c}_k$  and  $\mathbf{d}_k$ , all points in  $\mathbb{R}^3$ . Let  $\mathbf{x}_{k,j}$  be some point in  $\mathbb{R}^3$ , which will be common to the four tetrahedra that will be integrated over to obtain the integral over  $t_k$ . Although what follows applies for any point in  $\mathbb{R}^3$ , the point  $\mathbf{x}_{k,j}$  is an interpolation node from the set  $\mathcal{N}_k$  in this context. A unit length normal vector to the side of  $t_k$  with vertices  $\mathbf{a}_k$ ,  $\mathbf{b}_k$  and  $\mathbf{c}_k$  is defined by

$$\mathbf{n}_{\mathbf{a}_k \mathbf{b}_k \mathbf{c}_k} := \frac{(\mathbf{b}_k - \mathbf{a}_k) \times (\mathbf{c}_k - \mathbf{a}_k)}{\|(\mathbf{b}_k - \mathbf{a}_k) \times (\mathbf{c}_k - \mathbf{a}_k)\|_2},$$

and when defining a normal vector in what follows, the order of the vertices matters and should be taken as the order shown in this definition. Further, let  $\mathbf{e}_{k,j}$ ,  $\mathbf{f}_{k,j}$ ,  $\mathbf{g}_{k,j}$  and  $\mathbf{h}_{k,j}$  be the orthogonal projections of  $\mathbf{x}_{k,j}$  onto the faces of  $t_k$  with vertices  $\mathbf{a}_k$ ,  $\mathbf{b}_k$  and  $\mathbf{c}_k$ ;  $\mathbf{a}_k$ ,  $\mathbf{d}_k$  and  $\mathbf{b}_k$ ;  $\mathbf{a}_k$ ,  $\mathbf{c}_k$  and  $\mathbf{d}_k$ ; and  $\mathbf{b}_k$ ,  $\mathbf{d}_k$  and  $\mathbf{c}_k$ , respectively. For instance,

$$\mathbf{e}_{k,j} = \mathbf{x}_{k,j} + [(\mathbf{a}_k - \mathbf{x}_{k,j}) \cdot \mathbf{n}_{\mathbf{a}_k \mathbf{b}_k \mathbf{c}_k}] \mathbf{n}_{\mathbf{a}_k \mathbf{b}_k \mathbf{c}_k}, \quad (4)$$

Then by applying the divergence theorem it can be shown that

$$\begin{aligned} \iiint_{t_k} \phi(\|\mathbf{x} - \mathbf{x}_{k,j}\|_2) dV = & \\ & \left\{ \text{sign}((\mathbf{x}_{k,j} - \mathbf{e}_{k,j}) \cdot \mathbf{n}_{\mathbf{a}_k \mathbf{b}_k \mathbf{c}_k}) \iiint_{t_{\mathbf{x}_{k,j} \mathbf{a}_k \mathbf{b}_k \mathbf{c}_k}} \phi(\|\mathbf{x} - \mathbf{x}_{k,j}\|_2) + \cdots \right. \\ & \text{sign}((\mathbf{x}_{k,j} - \mathbf{f}_{k,j}) \cdot \mathbf{n}_{\mathbf{a}_k \mathbf{d}_k \mathbf{b}_k}) \iiint_{t_{\mathbf{x}_{k,j} \mathbf{a}_k \mathbf{d}_k \mathbf{b}_k}} \phi(\|\mathbf{x} - \mathbf{x}_{k,j}\|_2) + \cdots \\ & \text{sign}((\mathbf{x}_{k,j} - \mathbf{g}_{k,j}) \cdot \mathbf{n}_{\mathbf{a}_k \mathbf{c}_k \mathbf{d}_k}) \iiint_{t_{\mathbf{x}_{k,j} \mathbf{a}_k \mathbf{c}_k \mathbf{d}_k}} \phi(\|\mathbf{x} - \mathbf{x}_{k,j}\|_2) + \cdots \\ & \left. \text{sign}((\mathbf{x}_{k,j} - \mathbf{h}_{k,j}) \cdot \mathbf{n}_{\mathbf{b}_k \mathbf{d}_k \mathbf{c}_k}) \iiint_{t_{\mathbf{x}_{k,j} \mathbf{b}_k \mathbf{d}_k \mathbf{c}_k}} \phi(\|\mathbf{x} - \mathbf{x}_{k,j}\|_2) \right\}. \end{aligned}$$

This expression for the integral over  $t_k$  contains integrals over the four tetrahedra that share  $\mathbf{x}_{k,j}$  as a common vertex. Consider

$$\iiint_{t_{\mathbf{x}_{k,j} \mathbf{a}_k \mathbf{b}_k \mathbf{c}_k}} \phi(\|\mathbf{x} - \mathbf{x}_{k,j}\|_2) dV$$

since the remaining integrals over the tetrahedra are analogous. The integrand is radially symmetric about  $\mathbf{x}_{k,j}$  and depends only on the distance from  $\mathbf{x}_{k,j}$  suggesting the change of variables

$$\mathbf{x}(\sigma, \lambda_1, \lambda_2) = \mathbf{x}_{k,j} + \sigma(\lambda_1 \mathbf{a}_k + \lambda_2 \mathbf{b}_k + (1 - \lambda_1 - \lambda_2) \mathbf{c}_k - \mathbf{x}_{k,j}).$$

In this change of variables, it can be seen that triangles similar to, and parallel to, the side of  $t_k$  with vertices  $\mathbf{a}_k$ ,  $\mathbf{b}_k$  and  $\mathbf{c}_k$  are parameterized using barycentric coordinates and scaled by the nonnegative parameter  $\sigma$ , which accounts for the normalized distance of the point from the point  $\mathbf{x}_{k,j}$ . Under this change of variables the integral becomes

$$\int_0^1 \int_0^{1-\lambda_1} \int_0^1 \phi(\sigma \|\lambda_1 \mathbf{a}_k + \lambda_2 \mathbf{b}_k + (1 - \lambda_1 - \lambda_2) \mathbf{c}_k - \mathbf{x}_{k,j}\|_2) \sigma^2 V_{k,j} d\sigma d\lambda_2 d\lambda_1,$$

where  $V_{k,j} = |(\mathbf{a}_k - \mathbf{x}_{k,j}) \cdot [(\mathbf{b}_k - \mathbf{x}_{k,j}) \times (\mathbf{c}_k - \mathbf{x}_{k,j})]|$  is six times the volume of the tetrahedron  $t_{\mathbf{x}_{k,j} \mathbf{a}_k \mathbf{b}_k \mathbf{c}_k}$ . This volume appears in the Jacobian determinant from the change of variables.

Now, in the case of  $\phi(r) = r^{2p+1}$ ,  $p = 0, 1, 2, \dots$ , the iterated integrals in  $\sigma$  and then  $\lambda_2$  can be computed in closed form. However, exploring the integration over  $\lambda_1$  in Mathematica indicates the cost of a closed form expression for the integral is computationally too expensive, so the proposed algorithm uses standard pseudospectral methods for evaluating the integrals over  $\lambda_1$ .

### 2.3.2 Integrals Over Slivers of Volume at the Surface

When assigning a sliver of volume to a particular tetrahedron,  $t_k$ , care must be taken so that there are no gaps or overlaps between adjacent slivers. Let  $\tau_{k,i}$ ,  $i = 1, 2, 3, 4$ , be the triangular faces of  $t_k$ . At least one of these faces has all three vertices on the bounding surface. In most cases, this will be only one face of  $t_k$  (particularly when the volume is well resolved by small enough tetrahedra), call it  $\tau_{k,*}$ . In the case of the ball, as in [12], it turns out that if the three edges of  $\tau_{k,*}$  are projected radially from the center of the ball to the surface, gaps and overlaps will be prevented. Unfortunately this projection does not apply well to every bounded volume. For each edge of  $\tau_{k,*}$  an area between the edge of the triangle and a curve on the bounding surface constructed by projecting the edge to the surface is needed to form a side of the sliver of volume. The boundary of the sliver volume is formed by all three of these sides, the curved triangle on the bounding surface between the three sides, and the triangle  $\tau_{k,*}$ . Figure 1 illustrates one of these volumes.

To ensure that there are no gaps or overlaps, the procedure presented in [16] that is used to partition surfaces with a set of curved triangles is employed here. This procedure requires first locating a projection point ensuring that the triangular faces of each tetrahedron indexed by the set  $\mathcal{K}_S$  with three vertices on the bounding surface are not projected onto the same surface area and that the entire bounding surface is included in the union of the projections. The procedure for locating this projection point is reiterated in the following sections.

### 2.3.3 Defining the ‘‘Cutting’’ Plane

Locating the projection point for each triangle  $\tau_{k,*}$  begins by defining a unique ‘‘cutting’’ plane for each of its edges so that both of the two triangles containing a given edge, each likely the face of a different tetrahedron, will define the same plane.

Consider two triangles with vertices  $\mathbf{a}_{k,*}$ ,  $\mathbf{b}_{k,*}$  and  $\mathbf{c}_{k,*}$  and  $\mathbf{a}_{k,*}$ ,  $\mathbf{b}_{k,*}$  and  $\mathbf{e}_{k,*}$ , respectively. That is, these two triangles share the edge with vertices  $\mathbf{a}_{k,*}$  and  $\mathbf{b}_{k,*}$ . The cutting plane along the edge with vertices  $\mathbf{a}_{k,*}$  and  $\mathbf{b}_{k,*}$  is defined to contain the edge and to be parallel to the average of the normals  $\mathbf{n}_{\mathbf{a}_{k,*}\mathbf{b}_{k,*}\mathbf{c}_{k,*}}$  and  $\mathbf{n}_{\mathbf{a}_{k,*}\mathbf{b}_{k,*}\mathbf{e}_{k,*}}$  of the two triangles containing the edge pointing in the same general direction (that is, the angle between them is less than  $\frac{\pi}{2}$ ). This average vector is given by

$$\mathbf{n}_{\mathbf{a}_{k,*}\mathbf{b}_{k,*}} = \frac{1}{2} \left( \mathbf{n}_{\mathbf{a}_{k,*}\mathbf{b}_{k,*}\mathbf{c}_{k,*}} + \text{sign} \left( \mathbf{n}_{\mathbf{a}_{k,*}\mathbf{b}_{k,*}\mathbf{c}_{k,*}}^T \mathbf{n}_{\mathbf{a}_{k,*}\mathbf{b}_{k,*}\mathbf{e}_{k,*}} \right) \mathbf{n}_{\mathbf{a}_{k,*}\mathbf{b}_{k,*}\mathbf{e}_{k,*}} \right).$$

The vectors  $\mathbf{n}_{\mathbf{b}_{k,*}\mathbf{c}_{k,*}}$  and  $\mathbf{n}_{\mathbf{c}_{k,*}\mathbf{a}_{k,*}}$  can be defined similarly from the normal vectors to the triangles containing the appropriate edges.

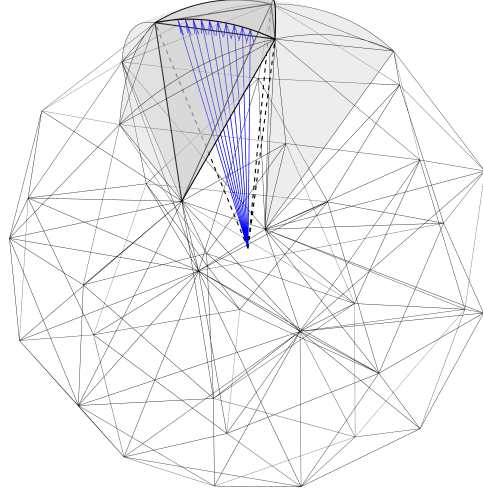


**Fig. 1** An illustration of the tetrahedra in the set  $T$ . The volume of one of the tetrahedra near the surface is outlined by thicker curves. Call the outlined tetrahedron  $t_k$  and let  $\tau_{k,*}$  be the face of  $t_k$  with three vertices on the surface of the sphere. The arrows indicate the projection of one of  $\tau_{k,*}$ 's edges to the surface from the origin. The dashed lines indicate the projection of  $\tau_{k,*}$ 's vertices from the origin. When decomposing the volume of the sphere, the area of the triangle  $\tau_{k,*}$ , the areas between the arcs on the sphere and the edges of  $\tau_{k,*}$  and the area of the spherical triangle between these arcs make of the boundary of the sliver of volume associated with  $t_k$ . The projection ensures that between adjacent slivers there are no gaps or overlaps, illustrated by the slivers of volume associated with three adjacent tetrahedra. This figure is adapted from [12].

#### 2.3.4 Locating a Projection Point

Once the three cutting planes have been defined for  $\tau_{k,*}$  the projection point, denoted  $\mathbf{p}_k$ , is taken as the intersection of the three cutting planes. These three planes will intersect at a single point in three dimensional space, except when the three edge normals  $\mathbf{n}_{\mathbf{a}_{k,*}\mathbf{b}_{k,*}}$ ,  $\mathbf{n}_{\mathbf{b}_{k,*}\mathbf{c}_{k,*}}$  and  $\mathbf{n}_{\mathbf{c}_{k,*}\mathbf{a}_{k,*}}$  are parallel. This point can be written as, for example,

$$\mathbf{p}_k = \mathbf{a}_{k,*} + \frac{\mathbf{n}_{\mathbf{p}_k\mathbf{b}_{k,*}\mathbf{c}_{k,*}} \cdot (\mathbf{b}_{k,*} - \mathbf{a}_{k,*})}{\mathbf{n}_{\mathbf{p}_k\mathbf{b}_{k,*}\mathbf{c}_{k,*}} \cdot \mathbf{v}_{\mathbf{p}_k\mathbf{a}_{k,*}}} \mathbf{v}_{\mathbf{p}_k\mathbf{a}_{k,*}}.$$

where  $\mathbf{n}_{\mathbf{p}_k\mathbf{a}_{k,*}\mathbf{b}_{k,*}} = \mathbf{n}_{\mathbf{a}_{k,*}\mathbf{b}_{k,*}} \times (\mathbf{b}_{k,*} - \mathbf{a}_{k,*})$ ,  $\mathbf{n}_{\mathbf{p}_k\mathbf{c}_{k,*}\mathbf{a}_{k,*}} = \mathbf{n}_{\mathbf{c}_{k,*}\mathbf{a}_{k,*}} \times (\mathbf{a}_{k,*} - \mathbf{c}_{k,*})$ , and

$$\mathbf{v}_{\mathbf{p}_k\mathbf{a}_{k,*}} = \mathbf{n}_{\mathbf{p}_k\mathbf{a}_{k,*}\mathbf{b}_{k,*}} \times \mathbf{n}_{\mathbf{p}_k\mathbf{c}_{k,*}\mathbf{a}_{k,*}},$$

with  $\times$  the vector cross product.

#### 2.3.5 Coordinate Transformation Via Projection

Assigning the slivers of volume via the projections from  $\mathbf{p}_k$  provides for a transformation of the coordinates of the sliver which allows the integral over its volume to be written as an iterated integral over a triangular area and a parameter,  $\sigma$ ,



which relates to the projection from  $\mathbf{p}_k$ . Consider any point  $\mathbf{x}$  in a neighborhood of the sliver volume. The line passing through  $\mathbf{p}_k$  and pointing in the direction of the vector  $\mathbf{x} - \mathbf{p}_k$  intersects the plane containing  $\tau_{k,*}$  at a point  $\mathbf{y}_{k,*}$  that is in the plane containing the triangle  $\tau_{k,*}$ . The point  $\mathbf{x}$  can therefore be represented as

$$\mathbf{x}(\lambda, \mu, \sigma) = \mathbf{y}_{k,*}(\lambda, \mu) + \sigma \mathbf{v}_{k,*}(\lambda, \mu), \quad (5)$$

where

$$\mathbf{v}_{k,*}(\lambda, \mu) = \frac{\mathbf{y}_{k,*}(\lambda, \mu) - \mathbf{p}_k}{\|\mathbf{y}_{k,*}(\lambda, \mu) - \mathbf{p}_k\|_2}$$

and  $\lambda$  and  $\mu$  define a two dimensional coordinate system for the plane containing  $\tau_{k,*}$ . For each value of  $\lambda$  and  $\mu$  the parameter  $\sigma$  ranges between 0 and  $\sigma_{\max}(\lambda, \mu)$ , where  $\sigma_{\max}(\lambda, \mu)$  is the smallest value of  $\sigma$  such that  $h(\mathbf{x}(\lambda, \mu, \sigma_{\max}(\lambda, \mu))) = 0$ ; that is,  $\mathbf{x}(\lambda, \mu, \sigma_{\max}(\lambda, \mu))$  is on the bounding surface. The value of  $\nu_k$  in (2) is defined as

$$\nu_k = \text{sign}((\mathbf{m}_k - \mathbf{m}_{k,*}) \cdot (\mathbf{p}_k - \mathbf{m}_{k,*}))$$

to ensure that only integrals over portions of  $s_k$  outside of  $t_k$  are added to the total volume and portions of  $s_k$  inside of  $t_k$  are subtracted given this choice of coordinate system. In this definition,  $\mathbf{m}_k$  and  $\mathbf{m}_{k,*}$  are the midpoints (average of the vertices) of the tetrahedron  $t_k$  and the triangle  $\tau_{k,*}$ , respectively.

Determining the value of  $\sigma_{\max}(\lambda, \mu)$  can be simple if the function  $h$  that defines the bounding surface is known and has roots that can be written in closed form. If the  $h$  is known but the roots cannot be written in closed form, then a rootfinding method such as Newton's method or Broyden's method [18] must be used to find the root,  $\sigma_{\max}(\lambda, \mu)$ , of  $h(\mathbf{x}(\lambda, \mu, \sigma_{\max}(\lambda, \mu))) = 0$  for each value of  $\lambda$  and  $\mu$  required to approximate the integral over the sliver volume. In either case, when  $h$  is known the parameterization of  $\tau_{k,*}$  via, for instance,

$$\mathbf{y}_{k,*}(\lambda, \mu) = (1 - \lambda)\mathbf{a}_{k,*} + \lambda((1 - \mu)\mathbf{b}_{k,*} + \mu\mathbf{c}_{k,*}) \quad (6)$$

where  $0 \leq \lambda \leq 1$  and  $0 \leq \mu \leq 1$ , allows the use of any number of quadrature techniques over intervals to evaluate the iterated integrals in

$$\iiint_{s_k} \phi(\|\mathbf{x} - \mathbf{x}_{k,j}\|) dV = \int_0^1 \int_0^1 \int_0^{\sigma_{\max}(\lambda, \mu)} \phi(\|\mathbf{x}(\lambda, \mu, \sigma) - \mathbf{x}_{k,j}\|) |J(\lambda, \mu, \sigma)| d\sigma d\lambda d\mu.$$

In the right hand side,

$$J(\lambda, \mu, \sigma) = \left(1 + \frac{\sigma}{\|\mathbf{y}_{k,*}(\lambda, \mu) - \mathbf{p}_k\|_2}\right)^2 \lambda [\mathbf{v}_{k,*}(\lambda, \mu) \cdot ((\mathbf{b}_{k,*} - \mathbf{a}_{k,*}) \times (\mathbf{c}_{k,*} - \mathbf{b}_{k,*}))]$$

is the Jacobian determinant of  $\mathbf{x}$  with respect to  $\sigma$ ,  $\lambda$  and  $\mu$ . On the other hand, if  $h$  is not known, a procedure for computing  $\sigma_{\max}(\lambda, \mu)$  and quadrature weights for evaluating the integrals in  $\lambda$  and  $\mu$  will be described in the following section. This procedure takes advantage of the knowledge that there are points in  $\mathcal{S}_N$  near  $\tau_{k,*}$ , including its vertices, that are also on the bounding surface. Once  $\sigma_{\max}(\lambda, \mu)$  is known at appropriate values of  $\lambda$  and  $\mu$ , the integral in  $\sigma$  can be easily treated with any number of quadrature methods over an interval. In the current implementation, a 21 node Legendre-Gauss-Lobatto quadrature rule is used for evaluating the integrals in each of  $\lambda$ ,  $\mu$  and  $\sigma$ .

## 2.4 Evaluating Integrals When the Implicit Parameterization of the Bounding Surface is Unknown

When  $h$  is unknown or unavailable, for instance, when the node set  $\mathcal{S}_N$  is determined by simulation or physical measurement, the value of  $\sigma_{\max}(\lambda, \mu)$  cannot be computed for most choices of  $\lambda$  and  $\mu$ . Therefore, a procedure is needed that allows the approximation of the integral over  $s_k$  using only points from  $\mathcal{S}_N$  that are located on the bounding surface where the upper bound on  $\sigma$  is directly computable.

Define a two dimensional coordinate system for the plane containing  $\tau_{k,*}$  via

$$\mathbf{y}_{k,*}(\lambda, \mu) = R_k^T \begin{bmatrix} \lambda \\ \mu \\ g_k \end{bmatrix} + \mathbf{p}_k,$$

where

$$g_k = |(\mathbf{m}_{k,*} - \mathbf{p}_k) \cdot \mathbf{n}_{\mathbf{a}_{k,*} \mathbf{b}_{k,*} \mathbf{c}_{k,*}}|,$$

$$\mathbf{m}_{k,*} = \frac{1}{3}(\mathbf{a}_{k,*} + \mathbf{b}_{k,*} + \mathbf{c}_{k,*})$$

and

$$R_k = \text{sign}(n_{k,x}) \text{sign}(n_{k,z}) \begin{bmatrix} \frac{n_{k,z} n_{k,x}}{\sqrt{n_{k,x}^2 + n_{k,y}^2}} & \frac{n_{k,z} n_{k,y}}{\sqrt{n_{k,x}^2 + n_{k,y}^2}} & -\frac{(n_{k,x}^2 + n_{k,y}^2)}{\sqrt{n_{k,x}^2 + n_{k,y}^2}} \\ -\frac{n_{k,y} \text{sign}(n_{k,z})}{\sqrt{n_{k,x}^2 + n_{k,y}^2}} & \frac{n_{k,x} \text{sign}(n_{k,z})}{\sqrt{n_{k,x}^2 + n_{k,y}^2}} & 0 \\ |n_{k,x}| & n_{k,y} \text{sign}(n_{k,x}) & n_{k,z} \text{sign}(n_{k,x}) \end{bmatrix},$$

with  $n_{k,x}$ ,  $n_{k,y}$  and  $n_{k,z}$  are the three components of  $\mathbf{n}_{\mathbf{a}_{k,*} \mathbf{b}_{k,*} \mathbf{c}_{k,*}}$ .

Let  $\mathcal{N}_{k,*} = \{\mathbf{x}_{k,*j}\}_{j=1}^{\eta}$  be the  $\eta$  points in  $\mathcal{S}_N$  nearest to the midpoint,  $\mathbf{m}_{k,*}$ , of  $\tau_{k,*}$  that also satisfy  $h(\mathbf{x}_{k,*j}) = 0$ . These are points exactly on the bounding surface. There is a point at the intersection of the plane containing  $\tau_{k,*}$  and the line segment connecting  $\mathbf{x}_{k,*j}$  and  $\mathbf{p}_k$  defined by

$$\mathbf{y}_{k,*j} = \mathbf{x}_{k,*j} - \frac{(\mathbf{x}_{k,*j} - \mathbf{m}_{k,*}) \cdot \mathbf{n}_{\mathbf{a}_{k,*} \mathbf{b}_{k,*} \mathbf{c}_{k,*}}}{(\mathbf{x}_{k,*j} - \mathbf{p}_k) \cdot \mathbf{n}_{\mathbf{a}_{k,*} \mathbf{b}_{k,*} \mathbf{c}_{k,*}}} (\mathbf{x}_{k,*j} - \mathbf{p}_k).$$

Denote the values of  $\lambda$  and  $\mu$  at these intersection points as  $\lambda_{k,j}$  and  $\mu_{k,j}$ , that is  $\mathbf{y}_{k,*}(\lambda_{k,j}, \mu_{k,j}) = \mathbf{y}_{k,*j}$  (and  $\mathbf{v}_{k,*}(\lambda_{k,j}, \mu_{k,j}) = \mathbf{v}_{k,*j}$ ), so that

$$\sigma_{\max}(\lambda_{k,j}, \mu_{k,j}) = \frac{(\mathbf{x}_{k,*j} - \mathbf{y}_{k,*j}) \cdot \mathbf{n}_{\mathbf{a}_{k,*} \mathbf{b}_{k,*} \mathbf{c}_{k,*}}}{\mathbf{v}_{k,*j} \cdot \mathbf{n}_{\mathbf{a}_{k,*} \mathbf{b}_{k,*} \mathbf{c}_{k,*}}}.$$

Now the integral over the sliver volume becomes

$$\iiint_{s_k} \phi(\|\mathbf{x} - \mathbf{x}_{k,j}\|) dV = \iint_{\tau_{k,*}} \int_0^{\sigma_{\max}(\lambda, \mu)} \phi(\|\mathbf{x}(\lambda, \mu, \sigma) - \mathbf{x}_{k,j}\|) |J(\lambda, \mu, \sigma)| d\sigma d\lambda d\mu,$$

with the Jacobian determinant now

$$J(\lambda, \mu, \sigma) = \left( 1 + \frac{\sigma}{\|\mathbf{y}_{k,*}(\lambda, \mu) - \mathbf{p}_k\|_2} \right)^2 [\mathbf{v}_{k,*}(\lambda, \mu) \cdot \mathbf{n}_{\mathbf{a}_{k,*} \mathbf{b}_{k,*} \mathbf{c}_{k,*}}].$$

In this expression the quadrature weights for approximating the integral over  $\tau_{k,*}$  can be found by now constructing a two dimensional RBF interpolant over the set of points  $\{(\lambda_{k,j}, \mu_{k,j})\}_{j=1}^{\eta}$  and integrating the interpolant, similar to what is presented in sections 2.2 and 2.3. In this case, the system of linear equations will require the RBFs and any bivariate polynomial terms included in the basis set to be integrated over the projection of  $\tau_{k,*}$  into the  $(\lambda, \mu)$  coordinate system. Closed form expressions for the integrals of the polynomial terms are easy to compute, and for many common RBFs closed form expressions also exist and can be computed as in [15,16,17]. The integral over  $\sigma$  can be approximated using any number of quadrature methods for an interval. In the current implementation, a 21 node Legendre-Gauss-Lobatto quadrature rule is used for evaluating the integral in  $\sigma$ .

#### 2.5 Step 4: Combine weights from the subdomains

Once the weights for each subdomain are computed, summing over all  $k \in \{1, 2, \dots, K\}$  leads to the approximation of the volume integral over  $\Omega$

$$\iiint_{\Omega} f(\mathbf{x}) dV \approx \sum_{k=1}^K \sum_{j=1}^n w_{k,j} f(\mathbf{x}_{k,j}).$$

Let  $\mathcal{K}_i$ ,  $i = 1, 2, \dots, N$ , be the set of all pairs  $(k, j)$  such that  $\mathbf{x}_{k,j} \mapsto \mathbf{x}_i$ . Then the volume integral over  $\Omega$  can be rewritten as

$$\iiint_{\Omega} f(\mathbf{x}) dV \approx \sum_{i=1}^N W_i f(\mathbf{x}_i). \quad (7)$$

### 3 Test Examples

To demonstrate the performance of the method describe in section 2, the algorithm was applied to three different test integrands featuring varying degrees of smoothness. Similar to the tests described in [16] and [17], weights are computed on quasi-uniformly spaced nodes bounded by a family of surfaces generated by rotating the Cassini ovals about the  $x$ -axis. That is, the bounding surfaces for these volumes are defined by the level surfaces

$$h(\mathbf{x}) = h(x, y, z) = (x^2 + y^2 + z^2)^2 - 2\alpha^2(x^2 - y^2 - z^2) + \alpha^4 - \beta^4 = 0, \quad (8)$$

which depend on the two parameters  $\alpha$  and  $\beta$ . The demonstrations here will consider  $\alpha = \lambda\beta$  for  $0 < \lambda < 1$  (specifically,  $\lambda = 0, 0.8, 0.95$ ). The parameter  $\beta$  in this work is chosen so that the volume is equal to 1, with  $\beta$  chosen numerically. Quadrature nodes for these volumes were generated using a modification of the algorithm presented in [19]. Examples of the node sets are displayed in figure 2.

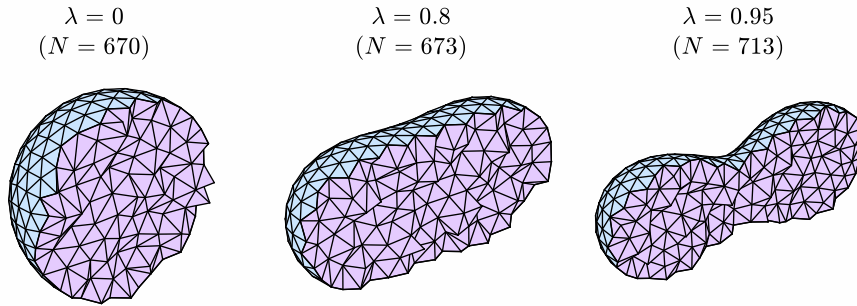


**Fig. 2** Examples of the quasi-uniformly spaced nodes in the volumes with bounding surfaces defined implicitly by (8).

### 3.1 Performance on Test Integrands

The algorithm was applied to three test integrands, first by utilizing the knowledge of the surface parameterization as in section 2.3.5 and second disregarding the known surface parameterization as in section 2.4. Just as in [12], when generating quadrature weights the radial basis function when constructing the interpolant on the *volume* was  $\phi(r) = r^3$  and the number of nearest neighbors,  $n = \frac{(m+1)(m+2)(m+3)}{3}$ , was based on the trivariate polynomial order  $m$ . The choice for  $n$  was guided by some computational experiments in, for instance, [17, 20, 21, 17] that indicated that in the presence of boundaries the number of nearest neighbors must be large enough to overcome effects like Runge phenomenon. The examples given in [17] indicated that the boundary errors were most prominent when nodes were (exactly) uniformly spaced, and the experiments in [12] suggested that this is a safe choice. When considering the case of an unknown bounding surface parameterization, the RBF chosen for integrals in the *plane* was  $r^7$  and the number of nearest neighbors was  $\eta = \lceil 1.05 \frac{(\gamma+1)(\gamma+2)}{2} \rceil$ . Here  $\gamma$  is the order of the bivariate polynomial included in the basis and in all cases  $\gamma = 2m$ . Given that the triangle to be integrated over is on the interior of the set of nodes used for interpolation, boundary effects pose less of a problem and the choice of  $\eta$  appears safe in this context.

The first of the test integrands is a degree 30 trivariate polynomial. That is, let

$$f_1(x, y, z) = \sum_{\alpha=0}^{30} \sum_{\beta=0}^{\alpha} \sum_{\gamma=0}^{\alpha-\beta} a_{\alpha\beta\gamma} x^{\alpha-\beta-\gamma} y^{\beta} z^{\gamma}.$$

Figures 3 and 4 display convergence of the approximate integral to the exact value at an order better than  $O(N^{-\frac{m}{3}})$ , where  $m$  corresponds to the order of the trivariate polynomial terms used in the approximation. If  $\Delta$  refers to a typical node separation distance, this corresponds to a convergence order of better than  $O(\Delta^m)$ , especially in the case of quasi-uniformly spaced nodes. The theory in [22]

explains that if the multivariate polynomial basis up to degree  $m$  is included in the process of RBF interpolation, then all of the terms in the Taylor series up to degree  $m$  will be handled exactly for the function being interpolated. The remaining terms in the Taylor series are then approximated by the RBF basis that was included. This is leading convergence at the order of at least  $O(\Delta^m)$ .

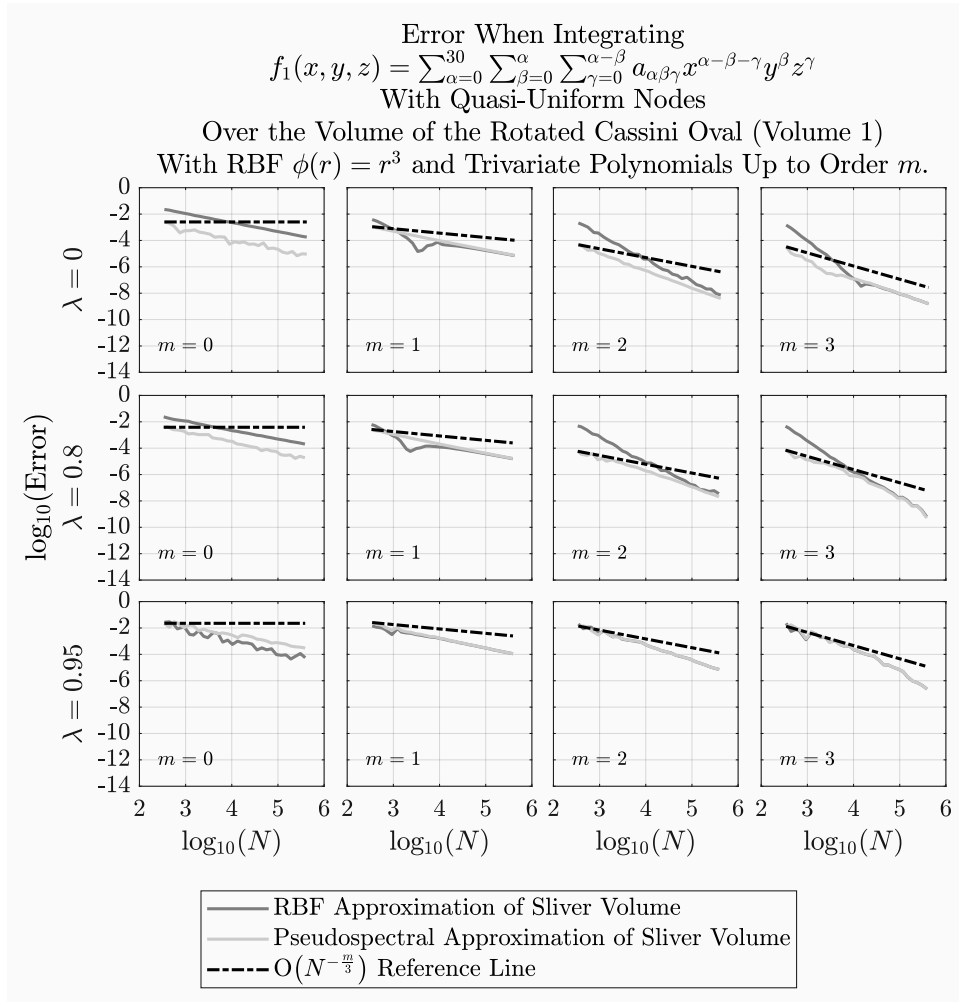


**Fig. 3** Log base 10 of the absolute error when approximating the volume integral of  $f_1$  over the test surfaces. The errors shown here are the largest after rotating the integrand 100 times about the  $x$ -axis. Notice that in many cases the error curve related to the RBF based approximation of the sliver volume is not visible as it lines up very closely with that of the pseudospectral approximation.

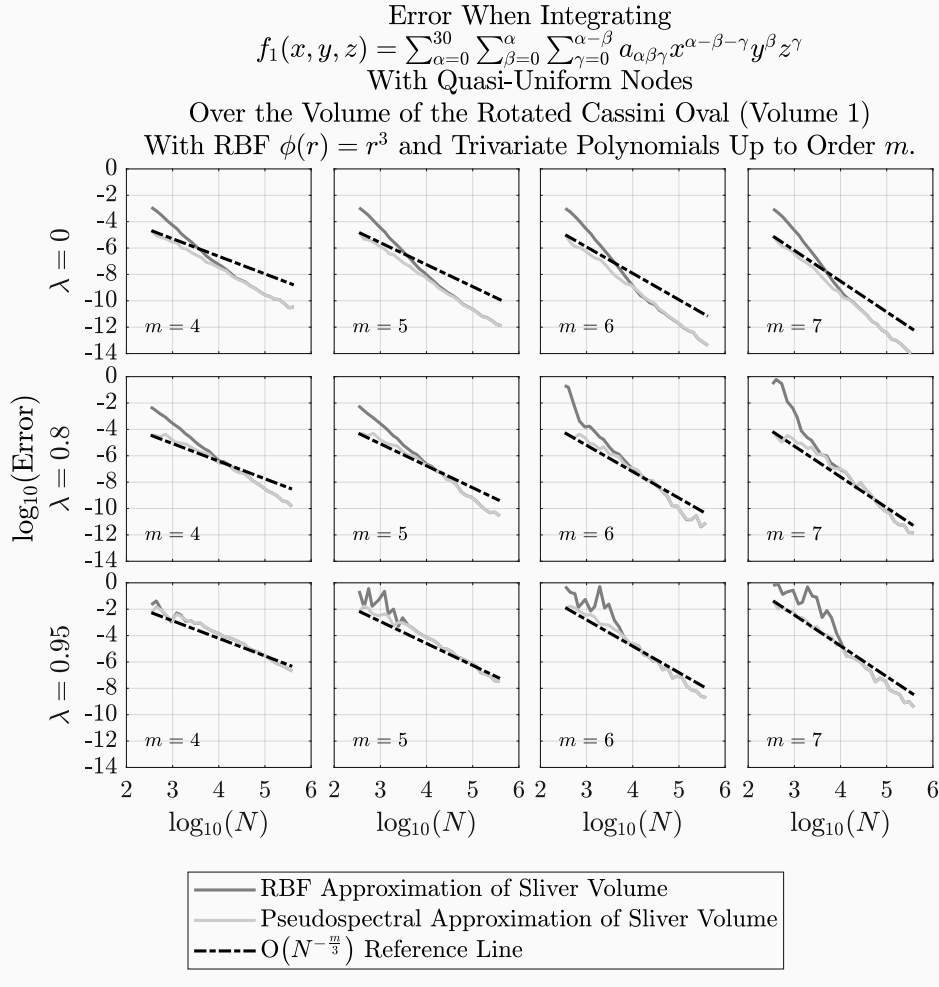


**Fig. 4** Log base 10 of the absolute error when approximating the volume integral of  $f_1$  over the test surfaces. The errors shown here are the largest after rotating the integrand 100 times about the  $x$ -axis. Notice that in many cases the error curve related to the RBF based approximation of the sliver volume is not visible as it lines up very closely with that of the pseudospectral approximation.

The second test integrand is the Gaussian

$$f_2(x, y, z) = \exp\left(-10\left((x - x_s)^2 + (y - y_s)^2 + (z - z_s)^2\right)\right)$$

where

$$(x_s, y_s, z_s) = (0.047056440432708, 0.071766893999009, 0.118950756342700)$$

is a randomly chosen shift of the center of the Gaussian from the origin. In order to have an accurate value to compare to, the volume integral was first approximated

by evaluating

$$\int_{-\beta\sqrt{1+\lambda^2}}^{\beta\sqrt{1+\lambda^2}} \int_{-\sqrt{\beta^4+4\beta^2\lambda^2x^2-x^2-\beta^2\lambda^2}}^{\sqrt{\beta^4+4\beta^2\lambda^2x^2-x^2-\beta^2\lambda^2}} \int_{-\sqrt{\beta^4+4\beta^2\lambda^2x^2-x^2-y^2-\beta^2\lambda^2}}^{\sqrt{\beta^4+4\beta^2\lambda^2x^2-x^2-y^2-\beta^2\lambda^2}} f_2(x, y, z) dz dy dx,$$

using Matlab's `integral3` command with the absolute and relative tolerances both set to ten times machine precision. Figures 5 and 6 illustrate the error in the integral of  $f_2$  over each volume when compared to the result from Matlab after rotating the integrand randomly 100 times about the  $x$ -axis. It is clear again that the order of the error is most dependent on the degree of the polynomials used in the interpolation.

The third test integrand is

$$f_3(x, y, z) = \text{sign}(z)$$

with `sign` the signum function. This function is discontinuous at the plane  $z = 0$ , so any method based on a continuous approximation of the integrand across the discontinuity should not be expected to achieve better than  $O(N^{-\frac{1}{3}})$  (i.e.  $O(\Delta)$ ) error. Figures 7 and 8 illustrate better than  $O(\Delta)$  error for the present method.

Finally, the algorithm was also applied to a test integrand featuring a steep and localized gradient. The test integrand was

$$f_4(x, y, z) = \tan^{-1}\left(5000(x^2 + y^2 + z^2)\right),$$

which has a steep gradient near the origin. Figures 9 and 10 illustrates that even with the steep and localized gradient the algorithm can perform with accuracy  $O(h^m)$ . The numerical tests in [12] suggest that node sets capturing the rapid change in the integrand can significantly improve the performance of the algorithm.

### 3.2 Computational Expense

Figure 11 illustrates the time to compute the set of quadrature weights on  $N$  nodes for various choice of the polynomial order,  $m$ . Consideration of each tetrahedron individually allows the time to compute a set of quadrature weights (and the use of memory) to scale like  $O(N)$ . This is in line with what is presented in [15,16,17,12]. Since the choice of  $m$  (and  $\mu$ ) affects the sizes of the systems of linear equations that need to be solved at each iteration, the figure shows an increase in the computational cost as  $m$  increases. These costs are also dependent on parameter choices for the quadrature rules used in sections 2.3.5 and 2.4 when integrating the three-dimensional RBF basis over the sliver volumes; however, the overall cost still scales as  $O(N)$ . Although parallelization tests are not presented for this specific algorithm, the results presented in [15] should translate to the algorithm proposed here. Except for the identification of nearest neighbors in order to construct the local weight set for each tetrahedron/sliver of volume and for the combination of weights in step 4 the algorithm is pleasingly parallel.

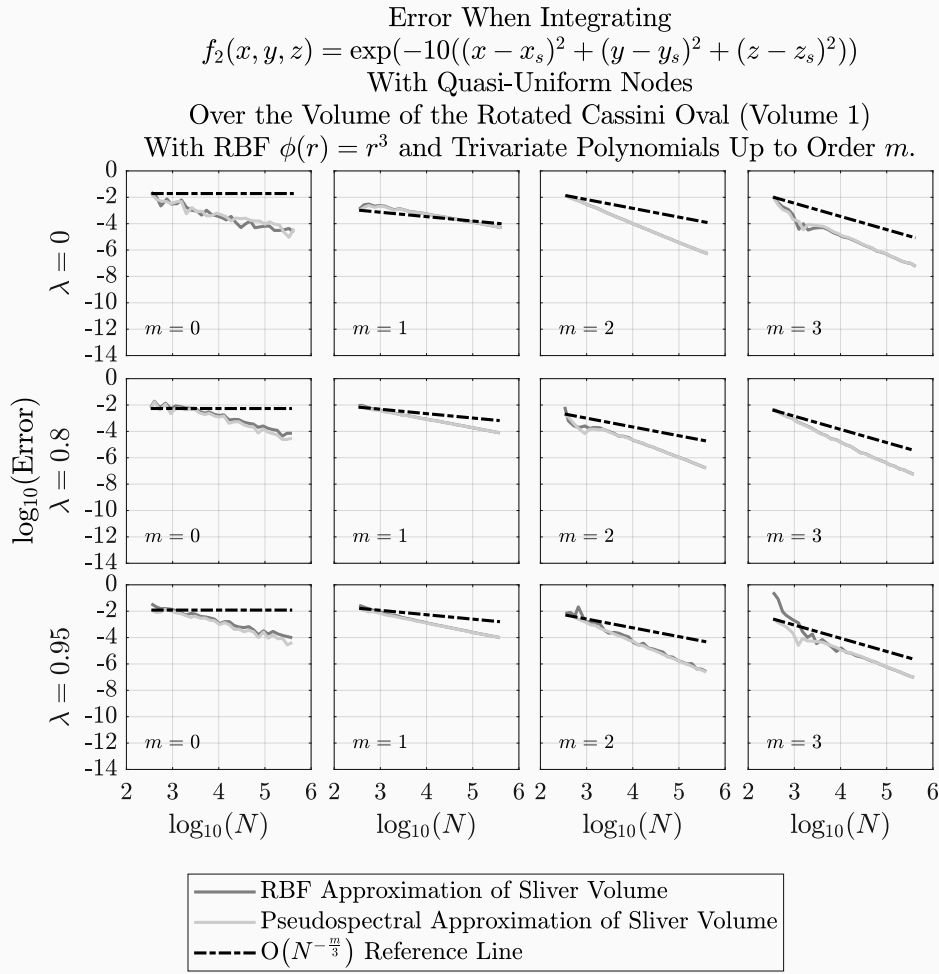


**Fig. 5** Log base 10 of the absolute error when approximating the volume integral of  $f_2$  over the test surfaces. The errors shown here are the largest after rotating the integrand 100 times about the  $x$ -axis. Notice that in many cases the error curve related to the RBF based approximation of the sliver volume is not visible as it lines up very closely with that of the pseudospectral approximation.

#### 4 Conclusions

This study has supplemented the previous RBF-FD based approach for evaluating definite integrals [15,16,17,12] with an extension to integrals over volumes bounded by smooth surfaces. The computational tests illustrate an algorithm that can achieve at least  $O(\Delta^m)$  accuracy, with  $\Delta$  the typical node separation distance and  $m$  the order of trivariate polynomial basis functions included in the approximation. On a set of  $N$  nodes in the volume, the computational cost is only  $O(N)$  and the algorithm is pleasingly parallel.



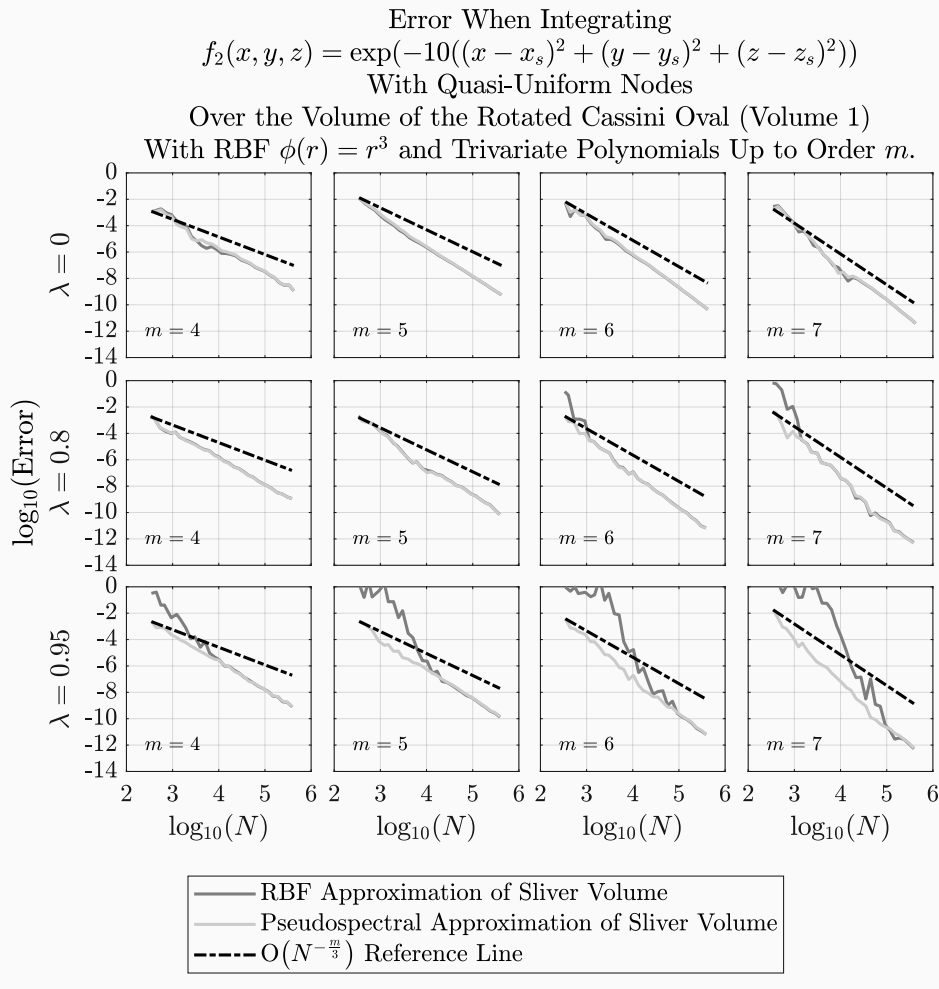


**Fig. 6** Log base 10 of the absolute error when approximating the volume integral of  $f_2$  over the test surfaces. The errors shown here are the largest after rotating the integrand 100 times about the  $x$ -axis. Notice that in many cases the error curve related to the RBF based approximation of the sliver volume is not visible as it lines up very closely with that of the pseudospectral approximation.

## References

1. W. Freeden and M. Gutting. *Integration and cubature methods: A geomathematically oriented course*. CRC Press, Boca Raton, Florida, United States, 2018.
2. A. H. Stroud. *Approximate calculation of multiple integrals*. Prentice-Hall, Inc., Englewood Cliffs, New Jersey, United States, 1971.
3. A. R. Krommer and C. W. Ueberhuber. *Computational integration*. SIAM, Philadelphia, Pennsylvania, United States, 1998.
4. P. K. Kytke and M. R. Schäferkötter. *Computational methods for integration*. Chapman & Hall/CRC, Boca Raton, Florida, United States, 2005.

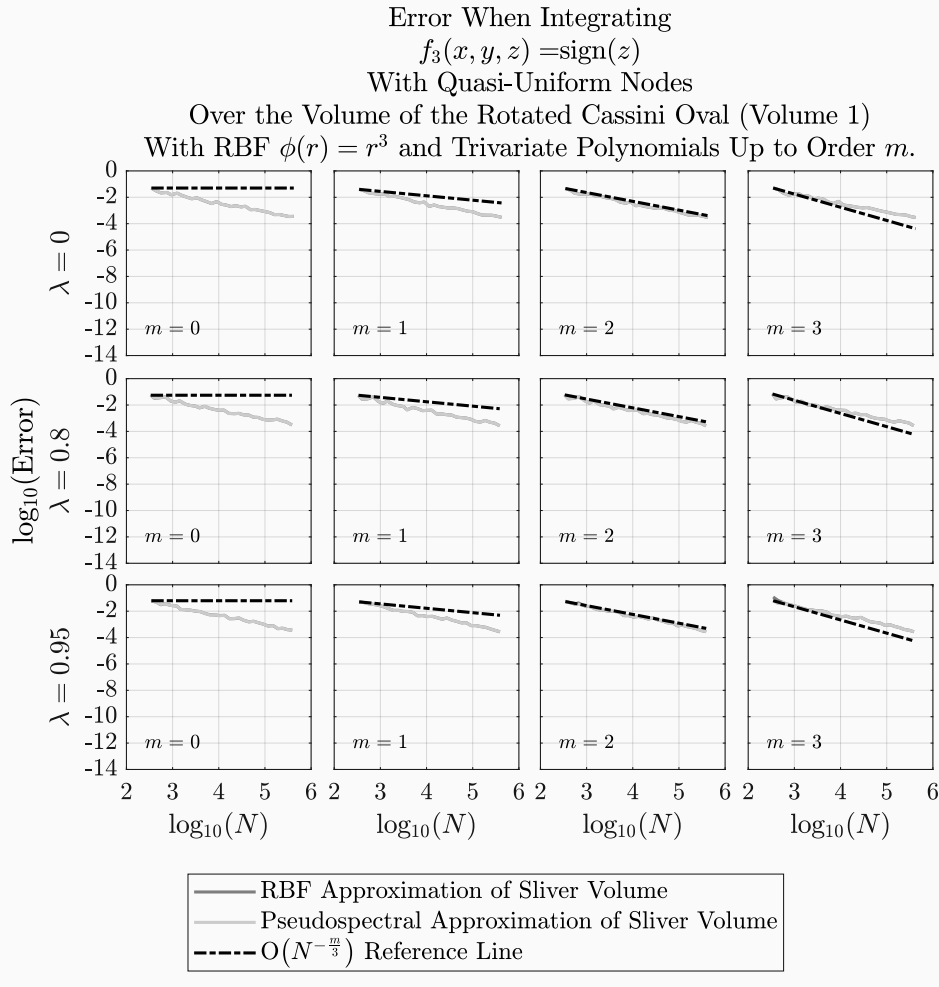


**Fig. 7** Log base 10 of the absolute error when approximating the volume integral of  $f_3$  over the test surfaces. The errors shown here are the largest after rotating the integrand 100 times about the  $x$ -axis. Notice that in many cases the error curve related to the RBF based approximation of the sliver volume is not visible as it lines up very closely with that of the pseudospectral approximation.

5. M. A. Olshanskii and D. Safin. Numerical integration over implicitly defined domains for higher order unfitted finite element methods. *Lobachevskii Journal of Mathematics*, 37:582—596.
6. R. I. Saye. High-order quadrature methods for implicitly defined surfaces and volumes in hyperrectangles. *SIAM J. Sci. Comput.*, 37(2):A993—A1019.
7. T. Cui, W. Leng, H. Liu, L. Zhang, and W. Zheng. High-order numerical quadratures in a tetrahedron with an implicitly defined curved interface. *ACM T. Math. Software*, 46(1):1–18.
8. B. Müller, F. Kummer, and M. Oberlack. Highly accurate surface and volume integration on implicit domains by means of moment-fitting. *Int. J. Numer. Meth. Eng.*, 96(8):512–528.

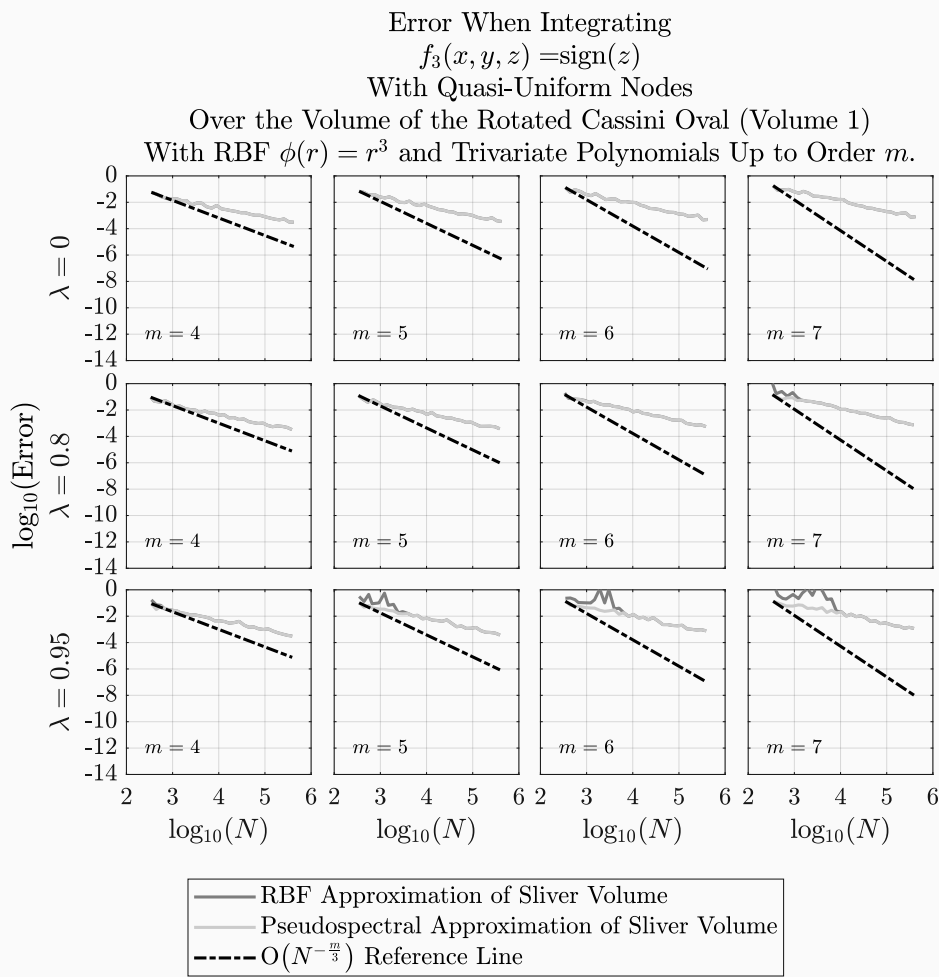


**Fig. 8** Log base 10 of the absolute error when approximating the volume integral of  $f_3$  over the test surfaces. The errors shown here are the largest after rotating the integrand 100 times about the  $x$ -axis. Notice that in many cases the error curve related to the RBF based approximation of the sliver volume is not visible as it lines up very closely with that of the pseudospectral approximation.

9. V. Keshavarzzadeh, R. M. Kirby, and A. Narayan. Numerical integration in multiple dimensions with designed quadrature. *SIAM J. Sci. Comput.*, 40(4):A2033–A2061.
10. Jr. P. C. Curtis.  $n$ -parameter families and best approximation. *Pacific J. Math*, 93:1013–1027, 1959.
11. J. C. Mairhuber. On Haar’s theorem concerning Chebyshev approximation problems having unique solutions. *Proc. Amer. Math. Soc.*, 7:609–615, 1956.
12. J. A. Reeger. Approximate integrals over the volume of the ball. *J. Sci Comput*, 83(45), 2020.
13. B. Fornberg and N. Flyer. Solving PDEs with radial basis functions. *Acta Numerica*, 24:215–258, 2015.

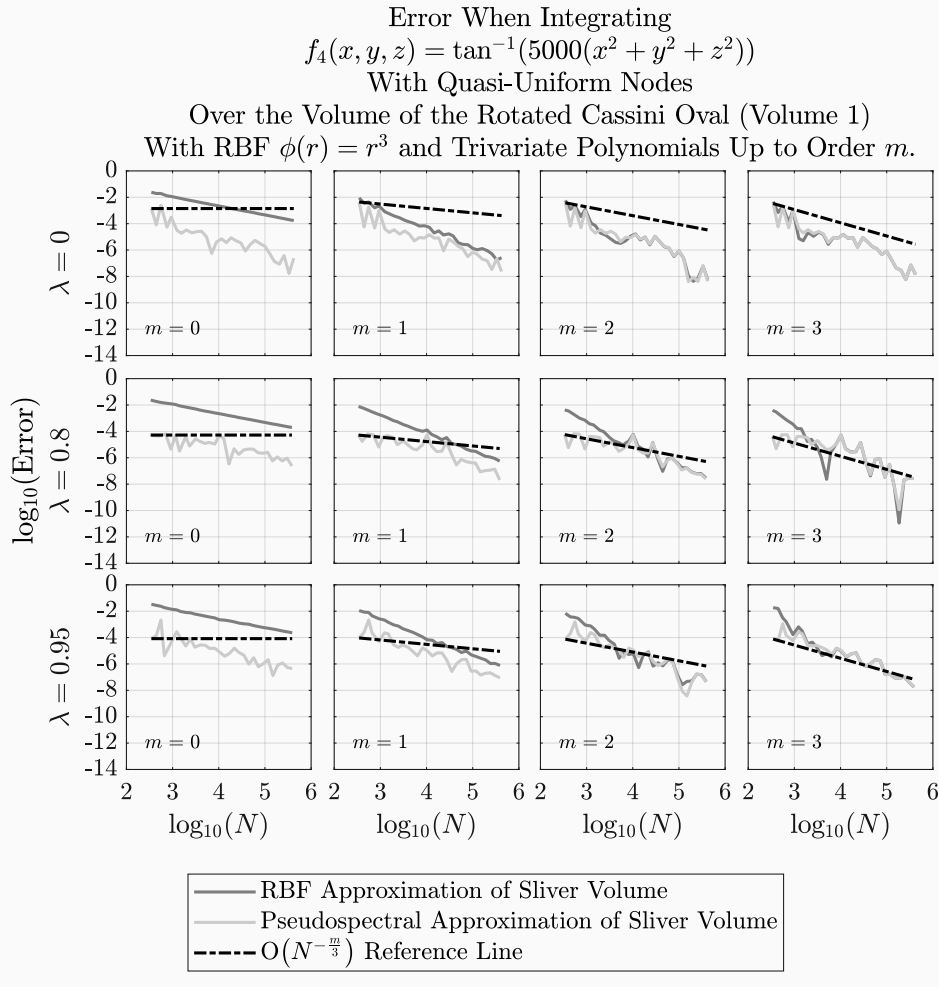


**Fig. 9** Log base 10 of the absolute error when approximating the volume integral of  $f_4$  over the test surfaces. The errors shown here are the largest after rotating the integrand 100 times about the  $x$ -axis. Notice that in some cases the error curve related to the RBF based approximation of the sliver volume is not visible as it lines up very closely with that of the pseudospectral approximation.

14. B. Fornberg and N. Flyer. *A primer on radial basis functions with applications to the geosciences*. SIAM, Philadelphia, U.S., 2015.
15. J. A. Reeger and B. Fornberg. Numerical quadrature over the surface of a sphere. *Stud. Appl. Math.*, 137(2):174–188, 2016.
16. J. A. Reeger, B. Fornberg, and M. L. Watts. Numerical quadrature over smooth, closed surfaces. *P. Roy. Soc. Lon. A Mat.*, 472, 2016. doi: 10.1098/rspa.2016.0401.
17. J. A. Reeger and B. Fornberg. Numerical quadrature over smooth surfaces with boundaries. *J. Comput. Phys.*, 355:176–190, 2018.
18. C. G. Broyden. A class of methods for solving nonlinear simultaneous equations. *Math. Comp.*, 19:577–593.

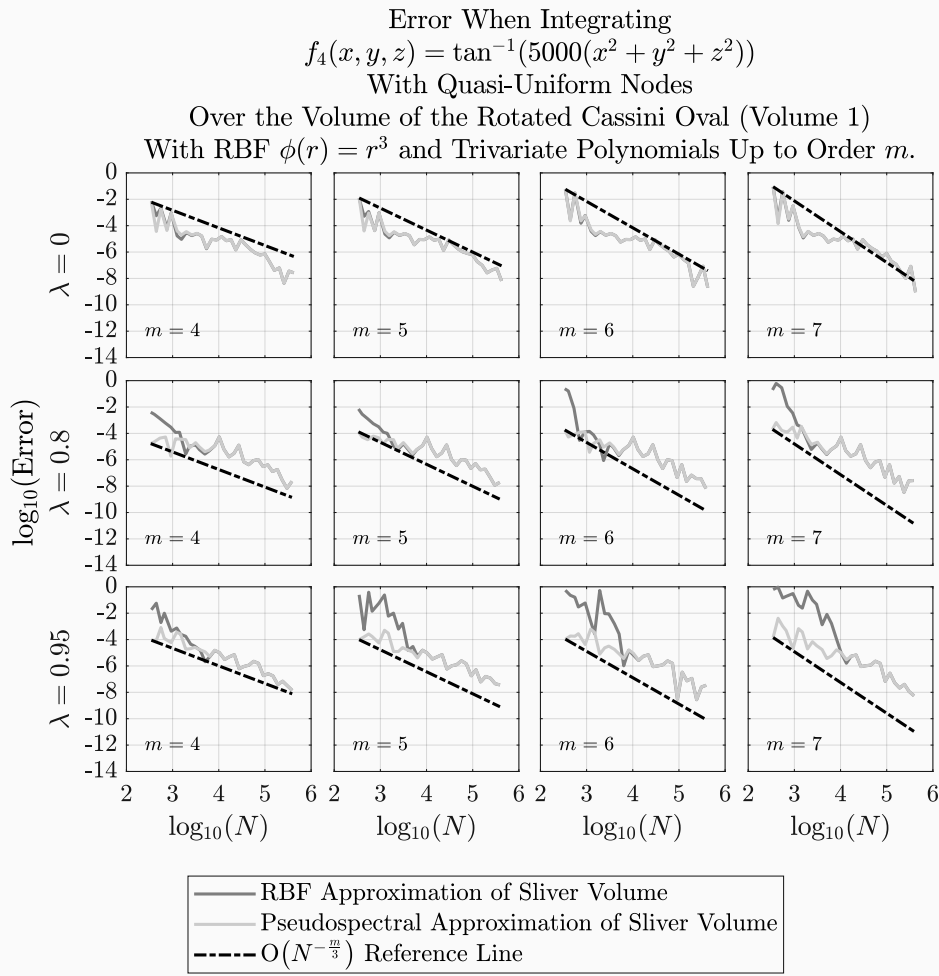


**Fig. 10** Log base 10 of the absolute error when approximating the volume integral of  $f_4$  over the test surfaces. The errors shown here are the largest after rotating the integrand 100 times about the  $x$ -axis. Notice that in some cases the error curve related to the RBF based approximation of the sliver volume is not visible as it lines up very closely with that of the pseudospectral approximation.

19. P. Persson and G. Strang. A simple mesh generator in Matlab. *SIAM Review*, 46(2):329–345, June 2004.
20. V. Bayona, N. Flyer, B. Fornberg, and G. A. Barnett. On the role of polynomials in RBF-FD approximations: II. Numerical solution of elliptic PDEs. *J. Comput. Phys.*, 332:257–273, 2017.
21. V. Bayona, N. Flyer, and B. Fornberg. On the role of polynomials in RBF-FD approximations: III. Behavior near domain boundaries. *J. Comput. Phys.*, 380:378–399, 2019.
22. V. Bayona. An insight into RBF-FD approximations augmented with polynomials. *Comput. Math. Appl.*, 77(9):2337–2353, 2019.

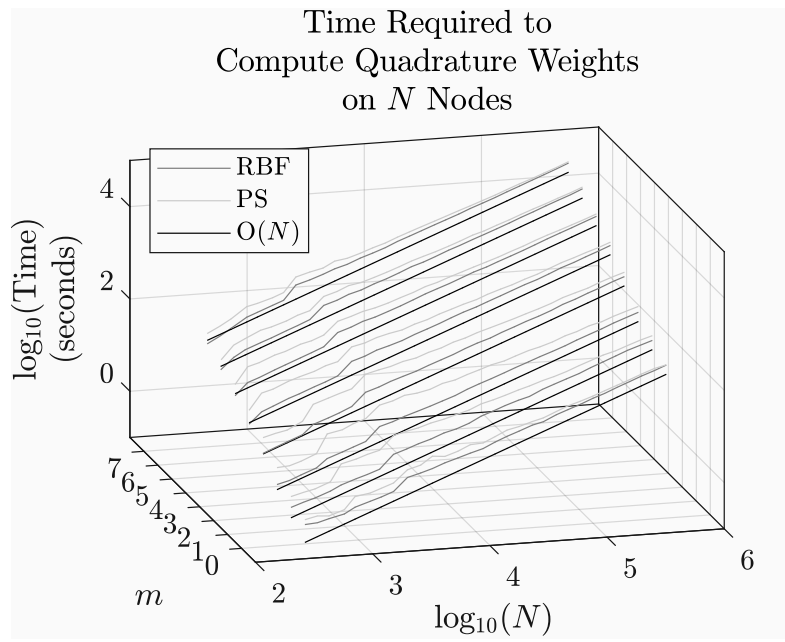


**Fig. 11** Log base 10 of the time it takes to compute quadrature weights on  $N$  nodes when including trivariate polynomial up to order  $m$ . The (black) dashed line is an  $O(N)$  reference line.